Letter

Optomechanically induced thermal bistability in an optical microresonator

Zhoutian Fu and Lan Yang*

Department of Electrical and Systems Engineering, Washington University, St. Louis, Missouri 63130, USA

(Received 15 December 2021; revised 1 June 2022; accepted 10 June 2022; published 30 June 2022)

Optomechanical systems have attracted considerable attention due to their wide applications in hybrid transduction systems, sensors, and quantum measurements. Classical optomechanical systems have various dynamical regimes that depend on the parameters, and the situation can be even more complicated when incorporated with other nonlinearities, such as the thermal nonlinearity that is common in optical resonators. Here, we experimentally and theoretically study the thermal bistability induced by optomechanical effect in a whispering-gallery mode microresonator. The mechanical oscillation modulates the intracavity photon number and modifies the thermal stability of states under a blue-detuned pump laser. Utilizing a silica microtip to suppress the mechanical motion, we identify the regions where the optical cavity temperature and detuning change due to the onset of oscillation and characterize the shifts in the detuning quantitatively. Hysteretic response in the mechanical frequency shifts (optical spring effect) to the pump wavelength is also observed to confirm the presence of bistability. The thermal dynamics discussed here is essentially different from the optomechanical heating and cooling of the effective temperature of the mechanical oscillator. This discovery shows that the thermal nonlinearity, which has been used for locking the pump frequency in the optomechanical systems, may also make some detuning states thermally unstable. Our study demonstrates an approach to characterize the detuning of the pump laser in an optomechanical resonator with thermal nonlinearity and also lays the groundwork for further understanding of dynamical effects induced by optomechanical effects.

DOI: 10.1103/PhysRevA.105.L061504

I. INTRODUCTION

In the past years, cavity optomechanics [1,2] have created many opportunities for fundamental studies and applications, ranging from ground-state cooling [3–5], quantum entanglement [6], optomechanically induced transparency [7,8], synchronization [9,10], chaos transfer [11], and sensing [12–18]. High-finesse optical cavities, such as the whispering-gallery mode (WGM) microresonators and photonic crystals, have been utilized to enhance the radiation force and realize a strong optomechanical coupling strength. One of the earliest observations of optomechanical effect in the microresonators is the mechanical self-oscillation excited by a blue-detuned pump laser [19], which can be constructed as a phonon laser that is analogous to photonic lasers [20,21]. Other dynamical states including limit torus, i.e., a state with multiple periods, chaos, and transient chaos have also been studied [11,22–24]. Since the presence of these states depends greatly on the parameter condition of the system [24], it is crucial to evaluate and monitor the system parameters in the experiments, especially when the optomechanical parametric instability and other types of nonlinearities coexist.

Thermal nonlinearity has proven to be one of the most ubiquitous nonlinear effects in high-quality (Q) microresonators. Typically, thermo-optic and thermal expansion effects are induced by strong photon absorption in the cavity, which can lead to nonlinear dynamical phenomena including thermal bistability [25] and thermal oscillation [26–28]. When optomechanical self-oscillation is excited, a relatively high optical power is often needed and consequently thermal nonlinearity also occurs in the microresonators. The intrinsic negative feedback provided by thermal effects has been utilized to lock the frequency of the pump laser [29,30], and thermally induced frequency shift can be used for the fine-tuning of resonance [9,21,31,32]. Moreover, there are many studies of the complex dynamics in the optomechanical systems with thermal nonlinearity. For example, a strong temperature gradient leads to nonuniform expansion in the device and gives rise to the photothermal force, which can drive the mechanical mode together with the radiation force [33–35]. If an additional type of nonlinearity, such as free-carrier dispersion and absorption, is considered, the system can exhibit a pulsatory state associated with a comblike structure in the frequency spectrum [36,37]. Recently, a new dynamical phenomenon called optomechanical thermo-oscillation is also observed, which happens as a result of competition between the slow thermal process and fast optomechanical oscillation [38]. The phenomena in these experiments only exist in a certain pump-detuning region, but detuning measurement is not straightforward in these systems due to nonlinearity. Therefore, a better understanding is needed of how detuning is altered in the situation that involves thermal nonlinearity and optomechanical oscillation.

Here, we study the interactions between the optomechanical effect and thermal nonlinearity within a silica WGM microtoroid. The mechanical oscillation induces an additional thermal bistability and leads to abrupt changes in detuning, which, in turn, affects the mechanical behaviors. We propose and demonstrate a method to characterize the detuning in

*yang@seas.wustl.edu

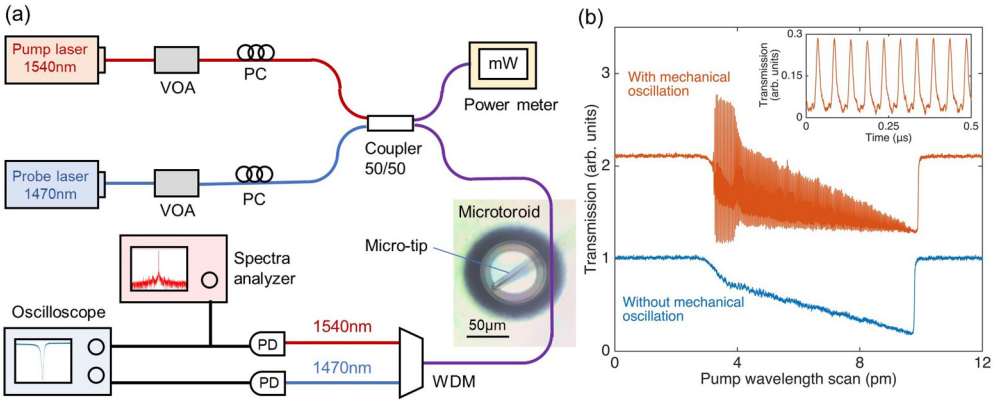

FIG. 1. (a) Schematic of the experiment setup. A single microtoroid is coupled to a fiber taper waveguide, and a silica microtip is used to suppress the mechanical oscillation. Two tunable lasers at 1540- and 1470-nm bands are used for pump and probe, respectively. VOA: variable optical attenuator, PC: polarization controller, WDM: wavelength division multiplexer, PD: photodetector. (b). Optical transmission spectra with mechanical oscillation switched on (orange line) and off (blue line) by the microtip. The microtip can suppress the mechanical motion of the microtoroid without affecting the optical mode and thermal broadening process. The inset shows a typical transmission modulated by the optomechanical effect.

the presence of mechanical oscillation in the blue-detuned side and identify the regions in which detuning will change with the onset of oscillation. Note that the detuning in our work is defined as the mismatch between the pump frequency and thermally shifted cavity resonance. The bistability is further confirmed by a hysteretic response in the mechanical frequency shifts to the pump wavelength. A model that incorporates the optical cavity mode, mechanical mode, and cavity temperature is developed to explain such thermal bistability: The intracavity photon number is modulated by the mechanical oscillation, and thus creates unstable thermal states in the blue-detuned side. This phenomenon universally exists in the microresonators with a strong optomechanical coupling strength and thermal nonlinearity.

II. RESULTS

The experiment setup for our study in the optomechanical system is shown in Fig. 1(a). The pump and probe lasers are coupled to a silica microtoroid via a fiber taper waveguide. The microtoroid supports a WGM in the 1540-nm wavelength band with an intrinsic linewidth $\kappa_0/2\pi = 5.23\,\mathrm{MHz}$, corresponding to an intrinsic Q factor of 3.7×10^7. To characterize the mechanical parameters of the microtoroid, the optical transmission signal at a low pump power is sent into a spectrum analyzer. The primary mechanical mode excited in our microtoroid is at a frequency of $\Omega_m/2\pi = 19.8\,\mathrm{MHz}$, with a linewidth of $\Gamma_m/2\pi = 28.3\,\mathrm{kHz}$. At a relatively high pump power, both optomechanical effect and thermal nonlinearity appear and the dynamical equations of the system are

$$\frac{d\alpha}{dt} = \left[i(\Delta_0 + \eta\delta T) - \frac{\kappa}{2}\right]\alpha + ig_{\mathrm{om}}(\beta + \beta^*)\alpha + \sqrt{\kappa_{\mathrm{ex}}}A_{\mathrm{in}}, \tag{1}$$

$$\frac{d\beta}{dt} = -\left(i\Omega_m + \frac{\Gamma_m}{2}\right)\beta + ig_{\mathrm{om}}|\alpha|^2, \tag{2}$$

$$\frac{d\delta T}{dt} = S|\alpha|^2 - \gamma_{th}\delta T, \tag{3}$$

where the amplitude of intracavity optical field α is normalized such that $|\alpha|^2$ equals the number of the intracavity photons. The optical mode has a total linewidth of κ and a resonance frequency ω_c when the cavity is cold (i.e., temperature change $\delta T = 0$). The cavity is driven by a blue-detuned pump laser with frequency ω_p and amplitude A_{in} under an external coupling $\kappa_{\mathrm{ex}}/2\pi = 12.5\,\mathrm{MHz}$, and $\Delta_0 = \omega_p - \omega_c$ is the detuning between the pump and cold cavity resonance frequency. The mechanical mode β is normalized such that the mechanical displacement is $x(t) = x_{\mathrm{ZPF}}(\beta + \beta^*)$, with $x_{\mathrm{ZPF}} = \sqrt{\hbar/(2m_{\mathrm{eff}}\Omega_m)}$ being the zero-point amplitude and m_{eff} being the effective mass of the microtoroid. The mechanical displacement alters the optical resonance frequency by $-g_{\mathrm{om}}(\beta + \beta^*)$. By characterizing the threshold power of mechanical self-oscillation, we are able to evaluate the coupling coefficient $g_{\mathrm{om}}/2\pi = 240\,\mathrm{Hz}$ and effective mass $m_{\mathrm{eff}} \approx 1.7 \times 10^{-10}\,\mathrm{g}$. The thermal effect in the cavity mainly consists of thermo-optic (dn/dT) and thermal expansion (dL/dT) of cavity length L, which leads to a linear frequency shift $-\eta\delta T$. Here, the temperature coefficient η can be explicitly expressed as $\eta = \omega_c(\frac{1}{n}\frac{dn}{dT} + \frac{1}{L}\frac{dL}{dT})$ and it is estimated to be $\eta/2\pi = 1.71\mathrm{GHz/K}$ [27]. From the thermally broadened optical transmission spectra, the thermal relaxation rate γ_{th} and heating rate per photon S can be obtained via parameter fitting, which yields $\gamma_{th} = 90\,\mathrm{kHz}$ and $S = 1.2 \times 10^{-4}\mathrm{K/s}$, respectively.

Figure 1(b) shows a typical optical transmission spectrum as we scan the pump wavelength forward, when mechanical oscillation and thermal nonlinearity coexist. The scanning rate is set to be 7.2 nm/s, which is slow enough for the optomechanical and thermal effects to behave adiabatically in our system. The pump power is fixed at 480 μW, and the mechanical motion in our study corresponds to a simple periodic limit cycle in the phase space. As the pump wavelength increases, the mechanical oscillation is strong initially but has an abrupt reduction in its amplitude at a certain point and then continues to diminish. The phenomenon is counterintuitive because we expect the variation of mechanical amplitude to follow the pattern of the optomechanical attractor diagram, which is a

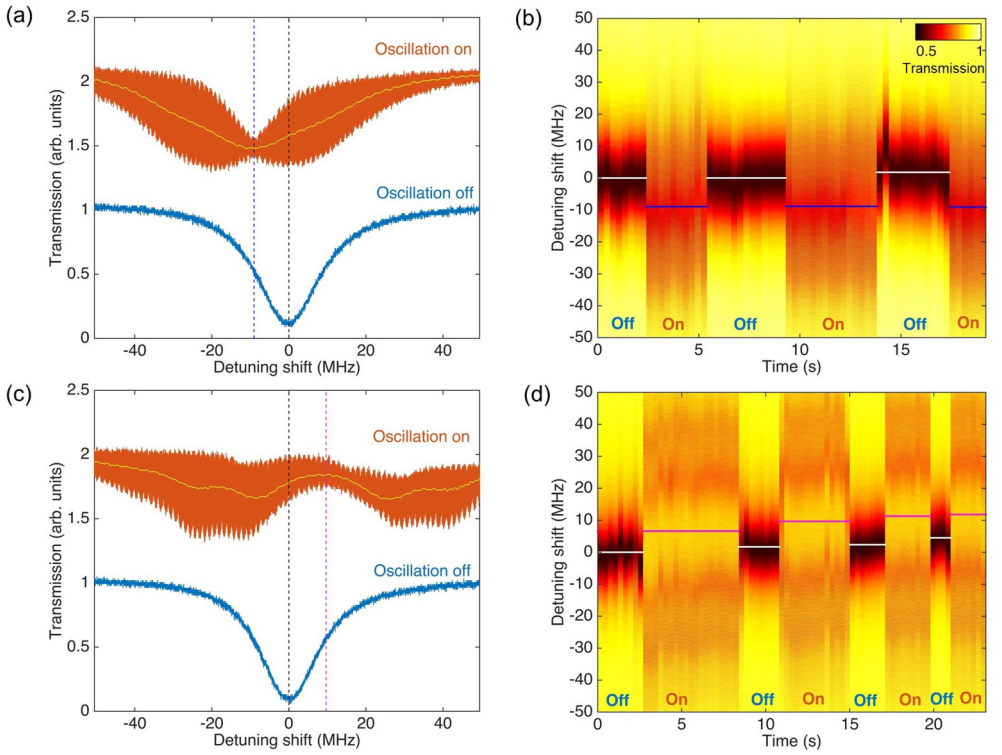

FIG. 2. (a), (c) Experimentally measured probe transmission spectra with mechanical oscillation turned on (orange line) and off (blue line) by a microtip at static detuning of 9.8 MHz (a) and 16.7 MHz (c), respectively. They are both processed by a 20-MHz built-in low-pass filter (LPF) of the oscilloscope to minimize the noise and higher harmonics. The yellow lines inside the orange ones are postprocessed by a 1-MHz LPF for the extraction of resonance (dashed lines). (b), (d) Temporal evolution of transmission spectra as we switch the oscillation on and off for multiple times in the experiments at static detuning of 9.8 MHz (b) and 16.7 MHz (d), respectively. Color scale indicates the optical transmission signal in an arbitrary unit. Solid horizontal lines represent the average resonance positions. The increase or decrease of detuning is consistent during the whole process that lasts for approximately 20 s.

smooth and wavy trajectory [39,40]. In the following sections, we will show that the reduction of amplitude actually indicates a change in the detuning.

The optomechanical effects on the detuning through thermal nonlinearity can be measured by switching the mechanical oscillation on and off using a fiber microtip. When a silica microtip with a diameter of several micrometers approaches the inner side of the ring, it suppresses the mechanical motion of the cavity but leaves the optical and thermal properties unperturbed. The thermal dissipation induced by the microtip is negligible because the thermal conductivity of silicon is two magnitudes larger than that of silica and, as a result, most heat dissipates to the silicon substrate rather than through the microtip (see the Supplemental Material [41]). Therefore, we can stop or release the mechanical oscillation at will by pressing the resonator with the microtip or moving it away.

To quantitatively monitor the thermal shift induced by the pump at a certain detuning, a low-power probe laser ($\sim$10 μW) at 1470-nm wavelength band is sent into the cavity. In the experiment, the pump frequency is locked while the probe frequency is scanned. Thus, the probe spectra provide the relative shifts of cavity resonance due to the pump-induced thermal effect, which can be used to evaluate the pump detuning changes. The probe and pump light are coupled to the same WGM but with different longitudinal orders, and they have the same Q factor, polarization dependence, and thermal property. Shown in Fig. 2(a), the blue curve is the probe transmission spectrum at a static detuning of 9.8 MHz, that is, the pump detuning without mechanical oscillation. With the mechanical oscillation on, the probe resonance has a frequency shift due to thermal effect and is also modulated. After applying a 1-MHz low-pass filter on the probe spectra, the cavity resonance change is readily extracted to be an increase of 9.0 MHz in this case. The temporal evolution of probe spectra as the oscillation is turned on and off several times is shown in Fig. 2(b), in which the change of resonance is confirmed to be consistent. Similarly, probe transmission spectra at a large static detuning of 16.7 MHz are shown in Fig. 2(c). Here, the mechanical oscillation has a much larger amplitude that modulates and deforms the observed probe WGM, but we are still able to extract resonance shift from the symmetric pattern under the low-pass filter. As a result, a consistent 9.6-MHz decrease of resonance frequency is observed whenever we switch on the oscillation [Fig. 2(d)].

Before theoretical analysis of the interplay between the mechanical oscillation and thermal nonlinearity, we need to first characterize the diagram of limit-cycle attractors in the optomechanical system only [39]. The thermal dynamical behavior is ignored temporarily and will be discussed later. This is done by solving Eq. (1) under the assumption that temperature shift is a static δT_0 and mechanical displacement

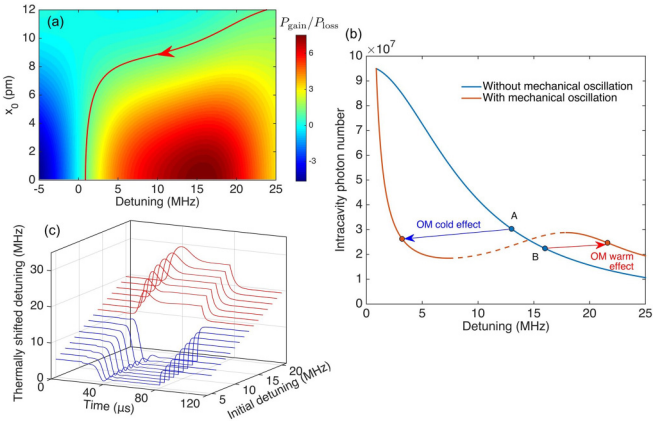

FIG. 3. (a) Theoretical attractor diagram in the space of mechanical oscillation amplitude x_0 and detuning. Color scale indicates the ratio of mechanical power gain from radiation pressure and loss due to frictions. The red line is the trajectory of stable attractors in the plane and the arrow is the forward direction of pump wavelength scanning in the experiment. (b) Detuning dependence of the average intracavity photon number with (orange line) and without mechanical oscillation (blue line). The former is calculated along the trajectory of attractors, which features a thermally unstable region in the middle (dashed line). Once mechanical motion starts, states at points A and B evolve differently due to optomechanical (OM) cold and warm effect, respectively. (c) Numerical simulations of the thermally shifted detuning, indicating OM warm and cold effects. With optomechanical coupling turned on and off at $t = 20\mu$s and $t = 80\ \mu$s, respectively, the thermally shifted detuning is recorded throughout the process, which shows the changes of steady-state temperature due to mechanical oscillation.

is $x(t) = \bar{x} + x_0 \cos(\Omega_m t)$. In this case, the solution of the optical amplitude is in the form of a Fourier series:

$$\alpha(t) = \sum_{n=-\infty}^{\infty} \frac{\sqrt{\kappa_{ex}} A_{in} J_n(-\theta)}{-i\bar{\Delta} + in\Omega_m + \kappa/2} \exp\left(in\Omega_m t + i\theta \sin(\Omega_m t)\right), \tag{4}$$

Where J_n is the Bessel function of the first kind and the detuning $\bar{\Delta} = \Delta_0 + \eta\delta T_0 + g_{om}\bar{x}/x_{ZPF}$. The argument of the Bessel function is defined as $\theta = g_{om}x_0/x_{ZPF}\Omega_m$. From the numerical simulations of Eqs. (1)–(3), it is found that the oscillation offset $\bar{x}$ is much smaller than the oscillation amplitude x_0 and is therefore ignored for the rest of derivation. With the optical amplitude expressed above, we can locate possible attractors of system dynamics by equating the mechanical power gain from radiation pressure $P_{gain} = \langle \hbar g_{om} |\alpha|^2 \dot{x}/x_{ZPF} \rangle$ and the power dissipation due to friction $P_{loss} = \Gamma_m m_{eff} \langle \dot{x}^2 \rangle$ [39]. This will lead to an equation that represents the instability condition for the mechanical oscillation:

$$\frac{2\hbar g_{om}}{\Gamma_m m_{eff} x_0 x_{ZPF} \Omega_m} \mathrm{Im}\left[\sum_n \alpha_n^*(x_0, \bar{\Delta})\alpha_{n+1}(x_0, \bar{\Delta})\right] = 1, \tag{5}$$

which describes the attractor diagram. Shown in Fig. 3(a), the stable attractors are plotted as the red line in the space of oscillation amplitude x_0 and detuning $\bar{\Delta}$ with the arrow indicating the forward direction of pump wavelength scanning.

The attractor diagram illustrates the relation between oscillation amplitude and detuning, but it does not contain the information about the thermal dynamics. It is therefore particularly important to know how mechanical oscillation affects the thermal steady state. To this end, we perform numerical simulations of time evolution of Eqs. (1)–(3), in which the optomechanical coupling is turned on and off and thermally shifted detuning is recorded through the process. At the initial state, the optomechanical coupling is set to be zero ($g_{om} = 0$) and the system is stationary at a detuning $\bar{\Delta}_{ini}$ with an initial temperature shift δT_{ini}, i.e., $\bar{\Delta}_{ini} = \Delta_0 + \eta\delta T_{ini}$. At a certain time ($t = 20\mu$s), the optomechanical coupling is turned on and mechanical oscillation appears. The thermal steady state of the cavity is found to be shifted as well, resulting in a change of the detuning. After the temperature becomes stable again, the optomechanical coupling is turned off at $t = 80\mu$s and the system will relax to the initial state as long as the thermal locking persists. Figure 3(c) shows the thermally shifted detuning $\bar{\Delta}(t) = \Delta_0 + \eta\delta T(t)$ in this process under different values of initial detuning. If the initial detuning is above a critical value (14 MHz in our parameter case), the onset of optomechanical coupling leads to an increase in temperature and thus increases the detuning; otherwise, it lowers the temperature as well as the detuning. Hence, these discoveries indicate that the increase and decrease of the cavity temperature are originated from the mechanical oscillation, termed optomechanical "warm" and "cold" effects, respectively. Note that these effects are essentially different from the heating and cooling effects caused by the radiation-pressure modified mechanical damping, because the former refers to a real temperature shift while the latter is about an effective temperature of the mechanical oscillator [42].

The aforementioned warm and cold effects exist because the mechanical oscillation modulates the intracavity photon number and changes the steady-state temperature. Since the oscillation (50 ns) is much faster than the thermal process ($\sim$11 μs), we only need to compare the time-averaged intracavity photon number $\bar{N} = \langle |\alpha(t)|^2 \rangle$ along the trajectories with and without mechanical oscillation in the attractor diagram (see the Supplemental Material [41]). Along these two trajectories, the dependence of average intracavity photon number with detuning is plotted in Fig. 3(b). We can see that the photon number is modulated by the mechanical oscillation, so its detuning dependence deviates from the standard Lorentzian line shape and has a secondary sideband. Therefore, if the modulated photon number is larger (smaller) than the unmodulated one, then it implies the presence of optomechanical coupling will result in a temperature rise (drop) and warm (cold) effect. For example, an initial state without oscillation at detuning $\bar{\Delta}/2\pi = 13$ MHz will evolve to the state at detuning $\bar{\Delta}/2\pi = 3.2$ MHz once optomechanical coupling is turned on, and similarly an initial state at $\bar{\Delta}/2\pi = 16$ MHz will evolve to $\bar{\Delta}/2\pi = 21.6$ MHz. The critical detuning between the regimes of warm and cold effects is $\bar{\Delta}_c/2\pi = 14.5$ MHz, which is the same as the transition point in the numerical simulations. It is also worth noting that there exists a thermally unstable region [25] in the presence of mechanical oscillation [dashed line in Fig. 3(b)]. As we scan the pump wavelength forward and backward, the system has two different stable thermal states in a certain region, which is essentially a thermal bistability induced by the optomechanical effect.

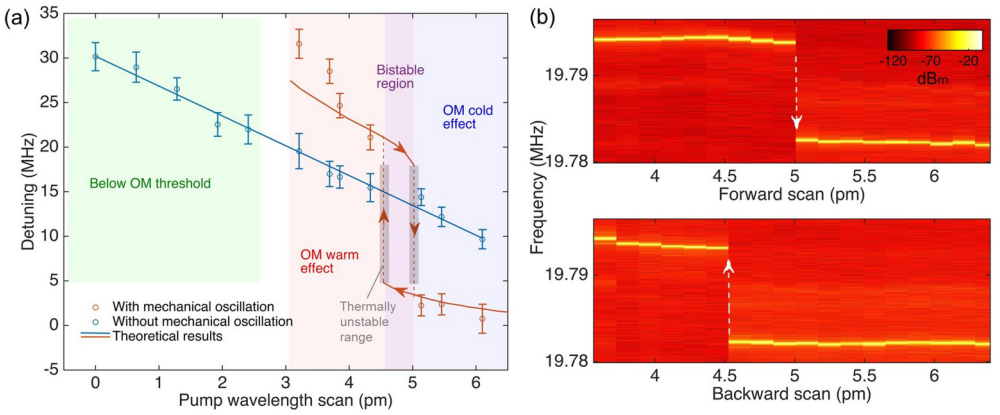

FIG. 4. (a) Detuning variation with and without mechanical oscillation as the pump wavelength increases. The detuning with mechanical oscillation is first larger than the static detuning (without oscillation), but at a certain point, it suddenly decreases to a very low level, which corresponds to the jump between two thermally stable states. The bistable region and the regions with OM warm and cold effects are marked in purple, pink, and blue shades, respectively. The thermally unstable detuning range (5 to 19 MHz) is marked in black shading. (b) Hysteretic response in the optomechanically induced thermal bistability, which manifests itself in the shift of mechanical frequency with respect to pump wavelength. Color scale indicates the mechanical spectra power in the unit of dBm.

In the experiment, the variation of detuning with and without mechanical oscillation as we continuously scan the pump wavelength forward is shown in Fig. 4(a), which illustrates the change of thermal steady states. In the case without mechanical oscillation (suppressed by the microtip), the detuning is determined by the thermal dynamics and continues to decrease in our system. However, the interaction of optomechanical and thermal effects can greatly alter the relation of detuning with respect to pump wavelength scanning. The mechanical oscillation is below threshold until the pump wavelength increases by around 2.6 pm from an off-resonance point with a 30-MHz detuning. Then, with the onset of mechanical oscillation, the detuning becomes substantially larger than that in the thermal-only case due to optomechanical warm effect. If the pump wavelength is further increased by 5 pm, the steady-state temperature drops significantly and detuning decreases below 5 MHz, which explains the amplitude reduction in Fig. 1(b). The error bars are calculated from multiple measurements and the error in this experiment mainly comes from the frequency stability of the probe and pump lasers. The theoretical results of detuning changes are also plotted in Fig. 4(a) and match well with the experiment data in the optomechanical cold-effect region. In the warm-effect region, the detuning measured in the experiments is slightly larger than the simulation results mainly because the mechanical oscillation is just above threshold and is not perfectly stable. The experiment results clearly show an inaccessible detuning range from 5 to 19 MHz due to the presence of the thermal bistability. This detuning range is inaccessible due to its thermally unstable state. A similar unstable state in an optomechanical system has also been briefly mentioned in the supplementary information of [38] but only with theoretical simulations. Our work has confirmed the phenomenon with experimental observations and theoretical analysis, and a method to evaluate detuning in this scenario has been proposed and demonstrated here. In this discussion, the mechanical oscillation is a simple periodic limit cycle in the phase space with a relatively small amplitude ($x_0 <$ 12 pm). However, the ideas of integrating thermal dynamics together with optomechanics [38,43] and the experimental method using a microtip can still be helpful to evaluate the detuning in a more complicated scenario, such as limit torus and chaotic cases [24].

Optomechanically induced thermal bistability also causes hysteresis as we do forward and backward scanning of the pump wavelength. In order to observe the hysteresis, we send the transmission signal of the pump to an electrical spectrum analyzer and monitor the changes in the mechanical frequency. In the forward and backward scan across the bistable region, the jump between the two states happens at different positions. Since the detuning is changed dramatically in the jump, there will be an abrupt shift of mechanical frequency due to optical spring effect [1]. In our experiment, we observed a 12-kHz frequency shift in the mechanical mode whenever the system crosses the bistable region [Fig. 4(b)]. The region of hysteresis is measured to be 0.5 pm long, conforming to the results in Fig. 4(a).

III. CONCLUSION

Our theoretical analysis based on attractor diagram shows that the mechanical oscillation modulates the average intracavity photon number and induces a thermal bistability under a blue-detuned pump laser. By using a microtip to suppress mechanical motion in a high-Q microresonator at will, we demonstrate that the onset of mechanical oscillation can alter the thermal steady state and thus the detuning: It can either raise the steady temperature to increase the detuning or lower the temperature and decrease the detuning. Hysteretic phenomenon in the mechanical frequency shifts is observed in the forward and backward pump wavelength scanning to further confirm the existence of bistability. Our results provide a guideline on the characterization of detuning variation in a blue-detuned optomechanical system and show the two sides of thermal effects: Thermal nonlinearity helps lock the pump frequency but may also make some detuning states unstable. The results improve our understanding of the dynamical states in the optomechanical systems, which can benefits

the applications such as non-Hermitian phonon lasers [21], optomechanical frequency comb [38,44], and self-organized synchronization [10].

ACKNOWLEDGMENT

This research was supported by the National Science Foundation (NSF Grant No. EFMA1641109).

[1] M. Aspelmeyer, T. J. Kippenberg, and F. Marquardt, Cavity optomechanics, Rev. Mod. Phys. **86**, 1391 (2014).
[2] T. J. Kippenberg and K. J. Vahala, Cavity optomechanics: Back-action at the mesoscale, Science **321**, 1172 (2008).
[3] A. Schliesser, R. Rivière, G. Anetsberger, O. Arcizet, and T. J. Kippenberg, Resolved-sideband cooling of a micromechanical oscillator, Nat. Phys. **4**, 415 (2008).
[4] A. Schliesser, O. Arcizet, R. Rivière, G. Anetsberger, and T. J. Kippenberg, Resolved-sideband cooling and position measurement of a micromechanical oscillator close to the Heisenberg uncertainty limit, Nat. Phys. **5**, 509 (2009).
[5] J. Chan, T. P. M. Alegre, A. H. Safavi-Naeini, J. T. Hill, A. Krause, S. Gröblacher, M. Aspelmeyer, and O. Painter, Laser cooling of a nanomechanical oscillator into its quantum ground state, Nature (London) **478**, 89 (2011).
[6] R. Riedinger, A. Wallucks, I. Marinković, C. Löschnauer, M. Aspelmeyer, S. Hong, and S. Gröblacher, Remote quantum entanglement between two micromechanical oscillators, Nature (London) **556**, 473 (2018).
[7] S. Weis, S. Deléglise, R. Rivière, E. Gavartin, O. Arcizet, A. Schliesser, and T. J. Kippenberg, Optomechanically induced transparency, Science **330**, 1520 (2010).
[8] A. H. Safavi-Naeini, T. P. M. Alegre, J. Chan, M. Eichenfield, M. Winger, Q. Lin, J. T. Hill, D. E. Chang, and O. Painter, Electromagnetically induced transparency and slow light with optomechanics, Nature (London) **472**, 69 (2011).
[9] M. Zhang, G. S. Wiederhecker, S. Manipatruni, A. Barnard, P. McEuen, and M. Lipson, Synchronization of Micromechanical Oscillators Using Light, Phys. Rev. Lett. **109**, 233906 (2012).
[10] J. Sheng, X. Wei, C. Yang, and H. Wu, Self-Organized Synchronization of Phonon Lasers, Phys. Rev. Lett. **124**, 053604 (2020).
[11] F. Monifi, J. Zhang, S. K. Özdemir, B. Peng, Y. X. Liu, F. Bo, F. Nori, and L. Yang, Optomechanically induced stochastic resonance and chaos transfer between optical fields, Nat. Photonics **10**, 399 (2016).
[12] A. G. Krause, M. Winger, T. D. Blasius, Q. Lin, and O. Painter, A high-resolution microchip optomechanical accelerometer, Nat. Photonics **6**, 768 (2012).
[13] J. Zhu, G. Zhao, I. Savukov, and L. Yang, Polymer encapsulated microcavity optomechanical magnetometer, Sci. Rep. **7**, 8896 (2017).
[14] B.-B. Li, J. Bílek, U. B. Hoff, L. S. Madsen, S. Forstner, V. Prakash, C. Schäfermeier, T. Gehring, W. P. Bowen, and U. L. Andersen, Quantum enhanced optomechanical magnetometry, Optica **5**, 850 (2018).
[15] W. Yu, W. C. Jiang, Q. Lin, and T. Lu, Cavity optomechanical spring sensing of single molecules, Nat. Commun. **7**, 12311 (2016).
[16] S. Basiri-Esfahani, A. Armin, S. Forstner, and W. P. Bowen, Precision ultrasound sensing on a chip, Nat. Commun. **10**, 132 (2019).
[17] E. Gil-Santos, J. J. Ruz, O. Malvar, I. Favero, A. Lemaître, P. M. Kosaka, S. García-López, M. Calleja, and J. Tamayo, Optomechanical detection of vibration modes of a single bacterium, Nat. Nanotechnol. **15**, 469 (2020).
[18] W. J. Westerveld, M. Mahmud-Ul-Hasan, R. Shnaiderman, V. Ntziachristos, X. Rottenberg, S. Severi, and V. Rochus, Sensitive, small, broadband and scalable optomechanical ultrasound sensor in silicon photonics, Nat. Photonics **15**, 341 (2021).
[19] T. Carmon, H. Rokhsari, L. Yang, T. J. Kippenberg, and K. J. Vahala, Temporal Behavior of Radiation-Pressure-Induced Vibrations of an Optical Microcavity Phonon Mode, Phys. Rev. Lett. **94**, 223902 (2005).
[20] I. S. Grudinin, H. Lee, O. Painter, and K. J. Vahala, Phonon Laser Action in a Tunable Two-Level System, Phys. Rev. Lett. **104**, 083901 (2010).
[21] J. Zhang, B. Peng, Ş. K. Özdemir, K. Pichler, D. O. Krimer, G. Zhao, F. Nori, Y. Liu, S. Rotter, and L. Yang, A phonon laser operating at an exceptional point, Nat. Photonics **12**, 479 (2018).
[22] L. Bakemeier, A. Alvermann, and H. Fehske, Route to Chaos in Optomechanics, Phys. Rev. Lett. **114**, 013601 (2015).
[23] D. Navarro-Urrios, N. E. Capuj, M. F. Colombano, P. D. Garciá, M. Sledzinska, F. Alzina, A. Griol, A. Martínez, and C. M. Sotomayor-Torres, Nonlinear dynamics and chaos in an optomechanical beam, Nat. Commun. **8**, 14965 (2017).
[24] T. F. Roque, F. Marquardt, and O. M. Yevtushenko, Nonlinear dynamics of weakly dissipative optomechanical systems, New J. Phys. **22**, 13049 (2020).
[25] T. Carmon, L. Yang, and K. J. Vahala, Dynamical thermal behavior and thermal self-stability of microcavities, Opt. Express **12**, 4742 (2004).
[26] A. E. Fomin, M. L. Gorodetsky, I. S. Grudinin, and V. S. Ilchenko, Nonstationary nonlinear effects in optical microspheres, J. Opt. Soc. Am. B **22**, 459 (2005).
[27] L. He, Y.-F. Xiao, J. Zhu, S. K. Ozdemir, and L. Yang, Oscillatory thermal dynamics in High-Q PDMS-coated silica toroidal microresonators, Opt. Express **17**, 9571 (2009).
[28] Z. C. Luo, C. Y. Ma, B. B. Li, and Y. F. Xiao, MHz-level self-sustained pulsation in polymer microspheres on a chip, AIP Adv. **4**, 122902 (2014).
[29] T. Carmon, T. J. Kippenberg, L. Yang, H. Rokhsari, S. Spillane, and K. J. Vahala, Feedback control of ultra-high-Q microcavities: Application to micro-Raman lasers and microparametric oscillators, Opt. Express **13**, 3558 (2005).
[30] T. G. McRae, K. H. Lee, M. McGovern, D. Gwyther, and W. P. Bowen, Thermo-optic locking of a semiconductor laser to a microcavity resonance, Opt. Express **17**, 21977 (2009).
[31] B. Peng, S. K. Özdemir, F. Lei, F. Monifi, M. Gianfreda, G. L. Long, S. Fan, F. Nori, C. M. Bender, and L. Yang, Parity-time-symmetric whispering-gallery microcavities, Nat. Phys. **10**, 394 (2014).

[32] B. Peng, S. K. Özdemir, S. Rotter, H. Yilmaz, M. Liertzer, F. Monifi, C. M. Bender, F. Nori, and L. Yang, Loss-induced suppression and revival of lasing, Science **346**, 328 (2014).

[33] M. W. Pruessner, T. H. Stievater, J. B. Khurgin, and W. S. Rabinovich, Integrated waveguide-DBR microcavity opto-mechanical system, Opt. Express **19**, 21904 (2011).

[34] D. Woolf, P.-C. Hui, E. Iwase, M. Khan, A. W. Rodriguez, P. Deotare, I. Bulu, S. G. Johnson, F. Capasso, and M. Loncar, Optomechanical and photothermal interactions in suspended photonic crystal membranes, Opt. Express **21**, 7258 (2013).

[35] B. D. Hauer, T. J. Clark, P. H. Kim, C. Doolin, and J. P. Davis, Dueling dynamical backaction in a cryogenic optomechanical cavity, Phys. Rev. A **99**, 053803 (2019).

[36] D. Navarro-Urrios, N. E. Capuj, J. Gomis-Bresco, F. Alzina, A. Pitanti, A. Griol, A. Martínez, and C. M. Sotomayor Torres, A self-stabilized coherent phonon source driven by optical forces, Sci. Rep. **5**, 15733 (2015).

[37] P. E. Allain, B. Guha, C. Baker, D. Parrain, A. Lemaître, G. Leo, and I. Favero, Electro-Optomechanical Modulation Instability in a Semiconductor Resonator, Phys. Rev. Lett. **126**, 243901 (2021).

[38] Y. Hu, S. Ding, Y. Qin, J. Gu, W. Wan, M. Xiao, and X. Jiang, Generation of Optical Frequency Comb Via Giant Optomechanical Oscillation, Phys. Rev. Lett. **127**, 134301 (2021).

[39] F. Marquardt, J. G. E. Harris, and S. M. Girvin, Dynamical Multistability Induced by Radiation Pressure in High-Finesse Micromechanical Optical Cavities, Phys. Rev. Lett. **96**, 103901 (2006).

[40] M. Ludwig, B. Kubala, and F. Marquardt, The optomechanical instability in the quantum regime, New J. Phys. **10**, 095013 (2008).

[41] See Supplemental Material at http://link.aps.org/supplemental/10.1103/PhysRevA.105.L061504 for the simulation of heat transfer in the system and the derivation of averaged intracavity photon number on the attractor diagram, which includes no additional reference.

[42] O. Arcizet, P. F. Cohadon, T. Briant, M. Pinard, and A. Heidmann, Radiation-pressure cooling and optomechanical instability of a micromirror, Nature (London) **444**, 71 (2006).

[43] A. G. Krause, J. T. Hill, M. Ludwig, A. H. Safavi-Naeini, J. Chan, F. Marquardt, and O. Painter, Nonlinear Radiation Pressure Dynamics in an Optomechanical Crystal, Phys. Rev. Lett. **115**, 233601 (2015).

[44] M. Miri, G. D. Aguanno, and A. Alù, Optomechanical frequency combs, New J. Phys. **20**, 043013 (2018).